Validation of an analytical optimization framework for wind farm wake steering applications

Ishaan Sood* and Johan Meyers†
KU Leuven, Celestijnenlaan 300, Leuven 3001, Belgium

Large-Eddy Simulations have been used extensively to develop and test wake steering wind farm control strategies through yaw control, however the high computational cost associated with these simulations makes studying wind farms operating under a large number of varying inflow conditions expensive. To this end, a fast Gaussian wake merging model has been developed at KU Leuven, which accounts for wake overlap between different turbines of a farm and enables rapid computations for performance analysis. In this work, we extend the wake model to include wake steering, and develop an optimization framework to determine yaw set-points across large wind farms for power maximization. The framework is tested on two wind farms for which normal operation data was already available to evaluate performance gains. The resulting set-points are then tested in an aeroelastic high-fidelity Large-Eddy Simulation solver, to verify the power gains and also analyze the structural impact of wake steering on turbine components. Results show that significant power gains up to 25% can be obtained through optimal wake steering, however at the cost of increase in fatigue damage on turbine components, thus decreasing the operational life of the turbines.

I. Introduction

Modern day wind farms suffer from energy extraction losses due to detrimental effects of wakes originating from upstream turbines rows on downstream rows. To overcome this, previous research has developed control strategies which either redirect turbine wakes through yaw misalignment or reduce wake strength by deviating from the optimal turbine axial induction set-points [1, 2]. Large Eddy Simulations have proven to be a valuable tool for developing and testing wake steering wind farm control strategies. However, the high computational cost associated with these simulations makes studying a large number of wake misalignment combinations expensive [3]. To this end, analytical wind farm simulation tools have gained popularity, as they enable rapid computations for a variety of inflow conditions [4]. In this work, we further extend an analytical wake steering model by incorporating it on a wind farm level, and combining with a recently developed recursive wake merging methodology [5]. The new model is then used to develop an optimization framework, which enables us to determine optimal yawing set-points for all the turbines in a farm for power maximization.

The present article is organized as follows : Section 2 details the model description, which includes the wind turbine wake model, the wake merging model and the developed optimization methodology for power optimization. In Section 3, the reference wind farm cases which are used for power optimization are detailed. Section 4 provides an overview of the LES framework utilized for validating the results from the analytical model, and the results are presented in section 5. Finally, the research findings and conclusions are given in section 6.

II. Model description

According to the Lanzilao wake merging model [5], if the wakes in the wind farm are assumed to be carried by the background flow $\boldsymbol{U}_b(\boldsymbol{x})$, the flow field in the farm can be evaluated using the recursive formula

$$\boldsymbol{U}_k(\boldsymbol{x}) = (\boldsymbol{U}_{k-1}(\boldsymbol{x}) \cdot \boldsymbol{e}_{\perp,i})(1 - W_k(\boldsymbol{x}))\boldsymbol{e}_{\perp,k} + (\boldsymbol{U}_{k-1}(\boldsymbol{x}) \cdot \boldsymbol{e}_{\parallel,k})\boldsymbol{e}_{\parallel,k}, \quad \text{for } k = 1, ..., N_t \tag{1}$$

The starting term of the recursion is given by $\boldsymbol{U}_o(\boldsymbol{x}) = \boldsymbol{U}_b(\boldsymbol{x})$, which is an input to the model. The final term in the recursion $\boldsymbol{U}_{N_t}$ is then the desired velocity profile throughout the wind farm. Unit vectors $\boldsymbol{e}_{\perp,k} = (cos\theta_k, sin\theta_k)$ and $\boldsymbol{e}_{\parallel,k} = (-sin\theta_k, cos\theta_k)$ account for the incoming wind direction and yaw angle at turbine k. The wake deficit W_k is evaluated using the Bastankhah model [4], according to which the wake deficit behind a yawed turbine is given by,

*PhD researcher, Department of Mechanical Engineering, KU Leuven, Celestijnenlaan 300, Leuven 3001, Belgium
†Professor, Department of Mechanical Engineering, KU Leuven, Celestijnenlaan 300, Leuven 3001, Belgium

$$W(x,y,z) = \left(1 - \sqrt{1 - \frac{C_T cos\gamma}{\frac{8\sigma_x\sigma_y}{D^2}})}\right) exp\left[-\frac{1}{2}\left\{\left(\frac{z-z_h}{\sigma_z}\right)^2 + \left(\frac{y-\delta}{\sigma_y}\right)^2\right\}\right] \tag{2}$$

Where, γ is the turbines yaw angle, C_T is the wind turbine thrust set-point coefficient and D is the turbine diameter. σ_y and σ_z are wake widths of the turbine at the downstream location which depend upon the incoming turbulence intensity *TI*, the wake deflection δ , and the downstream positions x, y and z. Further details of the model and its parameters can be found in the reference [4]. The total inflow velocity of the turbine k for the computation of its power is computed by averaging the velocity across the disc. To this end, we use the quadrature rule with $N_q = 16$ points, spread over the rotor disk. The quadrature-point coordinates are denoted by $x_{k,q}$ and are chosen following the rule proposed by Holoborodko with uniform weighting factor of $w_q = 1/N_q$ [6]. Hence, the disk average turbine inflow velocity can be determined by

$$U_k = \sum_{q=1}^{N_q} w_q S(x_{k,q}) \tag{3}$$

Where, S(x) = $||U(x)||_2$. Having computed the inflow velocities at each turbine, an optimization problem can be defined to maximize the total wind farm power prediction as follows

$$\begin{aligned} \min_{\boldsymbol{\gamma}} \quad & -1 * \sum_{k=1}^{N_t} \frac{1}{2}\rho C_P(\gamma_k) A_k U_k^3(\boldsymbol{\gamma}), \\ \text{s.t.} \quad & -\frac{\pi}{6} < \gamma < \frac{\pi}{6}. \end{aligned} \tag{4}$$

In the above equation, C_P is the coefficient of power of each turbine, evaluated for a yaw angle γ_k according to the cosine power law [7]. $\boldsymbol{\gamma}$ is a vector containing the yaw set points for all the turbines across the farm, $\boldsymbol{\gamma} = [\gamma_1, \gamma_2, ..., \gamma_{N_t}]$. The optimization problem is then solved to obtain optimal yaw angles for all the turbines within the wind farm using the SLSQP solver from the SciPy Python package, while utilizing the multi-start approach of basin-hopping to avoid local minima [8].

III. Optimization cases

Reference wind farm cases operating under normal operation are required to demonstrate the benefits of wake steering control. To this end, we make use of two different wind farm setups. For the first, we utilize the publicly available TotalControl reference wind farm database which comprises of numerical measurements obtained from LES spanning different atmospheric conditions and wind directions for the TotalContol Reference Wind Power Plant (TC RWP), which is a virtual wind farm comprising of 32 DTU 10 MW turbines, separated by 5D spacing in the vertical and horizontal directions [9]. Only the cases from the reference database with wind directions resulting in significant wake overlap between upstream and downstream turbines are considered for yaw optimization. The layout of the TC RWP is presented in Figure 1 (a).

The second wind farm under consideration for performance optimization through wake steering is the Lillgrund wind farm situated off the cost of Sweden. The wind farm comprises of 48 Siemens 2.3 MW turbines which are known to suffer from significant efficiency losses due to wake effects [10]. A comparison of the layout of the TC RWP and the Lillgrund wind farm is shown in Figure 1 (b). The reference cases used for the Lillgrund wind farm to determine the effect of wake steering are chosen from another TotalControl deliverable, D 1.2.1, in which data from a measurement campaign conducted at Lillgrund was used for validating an in-house LES code, SP-Wind. All the selected cases for optimization have been summarized in Table 1. *PDk* refers the Pressure Driven Boundary Layer (PDBL) simulations and *CNk2* and *CNk4* refer to Conventionally Neutral Boundary Layer (CNBL) simulations, with the suffix 2 and 4 denoting the strength of the capping inversion. Further details regarding the inflow database is available at the publicly available TotalControl inflow database [11–14]. The inflows PDk_1, PDk_2 and , PDk_3 are flow-fields obtained by scaling and shifting the *PDk* inflow, achieved by changing the surface roughness and friction velocity to match the inflow conditions at the Lillgrund wind farm during the measurement campaign. Therefore, 8 references cases spanning the two wind farms and different inflow conditions are available for wind farm power optimization, for which the optimal yaw set-points are determined through the framework described in the previous section. Free stream wind velocity and

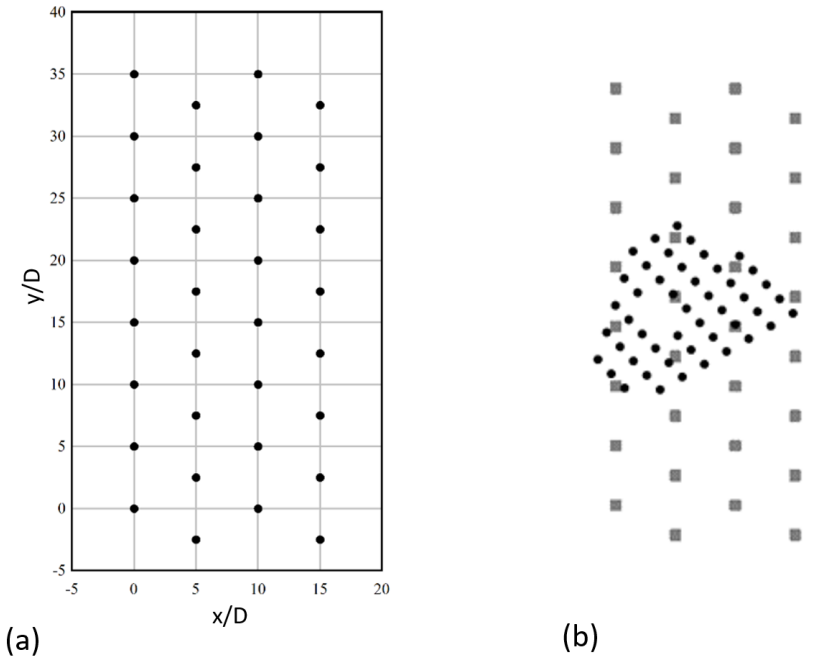

Fig. 1 (a) Layout of the TC RWP with a rotor diameter D = 178.3 m**. (b) Scale comparison of the TC RWP (gray) and the Lillgrund wind farm (black). Lillgrund turbines have a rotor diameter of D =** 93 m

turbulence intensity at turbine hub height, which are input parameters required for the wake model, are obtained from the respective flow profile from the reference LES database. The resulting yaw set-points for all the cases are presented in Figure 2. From results of the optimizations, it can be observed that cases which had fully aligned turbines, such as cases 1,5 and 6, tend to have the largest yaw set-points to steer the wake away from the fully waked downstream turbines. Cases with staggered turbines, such as cases 3 and 7, have lower optimal yaw set-points due to the limited available space for wake steering without causing further wake overlaps, hence reduction in farm power output.

IV. LES validation framework

To validate the performance gains through optimal wake steering, the yaw set-points obtained from the optimizations are used as inputs for simulations in a LES environment using the SP-Wind framework, which has extensively been used in the past years for wind farm simulations [15–17]. Using SP-Wind, the three-dimensional, unsteady, and spatially filtered Navier-Stokes momentum and temperature equations

$$\frac{\partial \tilde{\mathbf{u}}}{\partial t} + (\tilde{\mathbf{u}} \cdot \nabla)\tilde{\mathbf{u}} = -\frac{\nabla(\tilde{p} + p_\infty)}{\rho} - \nabla \cdot \boldsymbol{\tau_s} + 2\boldsymbol{\omega} \times \tilde{\mathbf{u}} + g\frac{(\tilde{\theta} - \theta_0)}{\theta_0} + \bar{\mathbf{F}} \tag{5}$$

$$\frac{\partial \tilde{\theta}}{\partial t} + (\tilde{\mathbf{u}} \cdot \nabla)\tilde{\theta} = -\nabla \cdot \boldsymbol{q_s} \tag{6}$$

are solved. $\tilde{\mathbf{u}} = [\tilde{u_1}, \tilde{u_2}, \tilde{u_3}]$ is the filtered velocity field, $\tilde{\theta}$ is the filtered potential temperature field, and θ_0 is the background adiabatic base state. The pressure gradient is split into a mean background pressure gradient ∇p_∞ driving the mean flow, and a fluctuating component $\nabla \tilde{p}$. The very high Reynolds numbers in the atmospheric boundary-layer flow combined with typical spatial resolutions in LES justify the omission of resolved effects of viscous momentum transfer and diffusive heat transfer. Instead, these are represented by modeling the subgrid-scale stress tensor $\boldsymbol{\tau_s}$ and the subgrid-scale heat flux q_s originating from spatially filtering the governing equations [18]. Coriolis effects are included through the angular velocity vector $\boldsymbol{\omega} = \Omega sin\phi$, where Ω is the earth's rotation and ϕ is the latitude of the wind farm. $g(\tilde{\theta} - \theta_0)/\theta_0$ represents thermal buoyancy, with g the gravitational acceleration, $\tilde{\theta}$ the filtered potential temperature

Table 1 Specifications of the reference database

Case No.	Inflow	Wind farm	Wind direction	Hub height wind speed	Hub height TI
1	*PDk*	TC RWP	0°	9.4 m s^{-1}	5.15%
2	*CNk2*	TC RWP	300°	11.0 m s^{-1}	3.66%
3	*CNk2*	TC RWP	330°	11.0 m s^{-1}	3.66%
4	*CNk4*	TC RWP	300°	11.3 m s^{-1}	3.65%
5	*CNk4*	TC RWP	0°	11.3 m s^{-1}	3.65%
6	PDk_1	Lillgrund	119°	8.2 m s^{-1}	6.31%
7	PDk_2	Lillgrund	243°	8.5 m s^{-1}	6.27%
8	PDk_3	Lillgrund	110°	4.8 m s^{-1}	6.83%

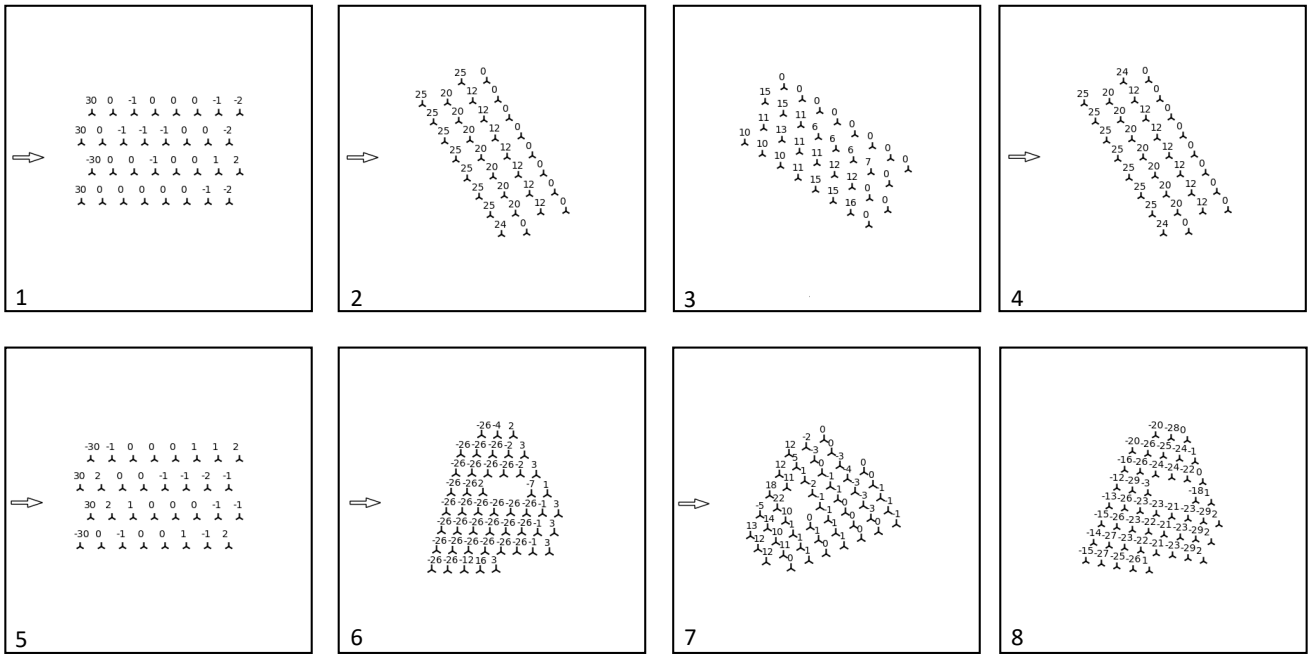

Fig. 2 Optimal yawing set-points obtained for the 8 reference cases. Cases 1 - 5 are for the TCRWP, cases 6-8 are for the Lillgrund wind farm.

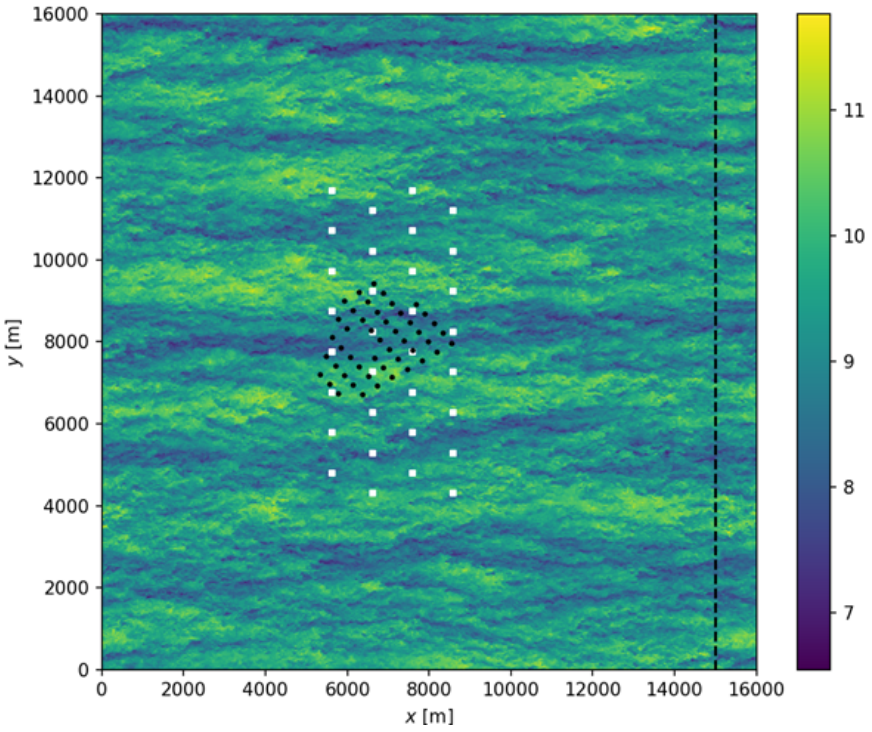

Fig. 3 Planview of Lillgrund (black) and TC RWP (white) in simulation domain. The black dashed line indicates the extent of the slab from which inflow data is extracted from the precursor domain (without turbines). The background is coloured with a typical instantaneous stream-wise velocity field at hub-height in a precursor simulation without turbines

Table 2 Summary of the general domain and time parameters

Domain size	$L_x \times L_y \times L_z$	$16 \times 16 \times 1.5$ km
Grid	$N_x \times N_y \times N_z$	$1200 \times 1200 \times 225$
Resolution	$\Delta_x \times \Delta_y \times \Delta_z$	$13.33 \times 13.33 \times 6.66$ m
wind farm spin-up time	T_{spin}	15 min
Simulation time	T	60 min
LES time step	Δt_{LES}	0.5 s
Structural time step	Δt_{MBS}	0.01 s

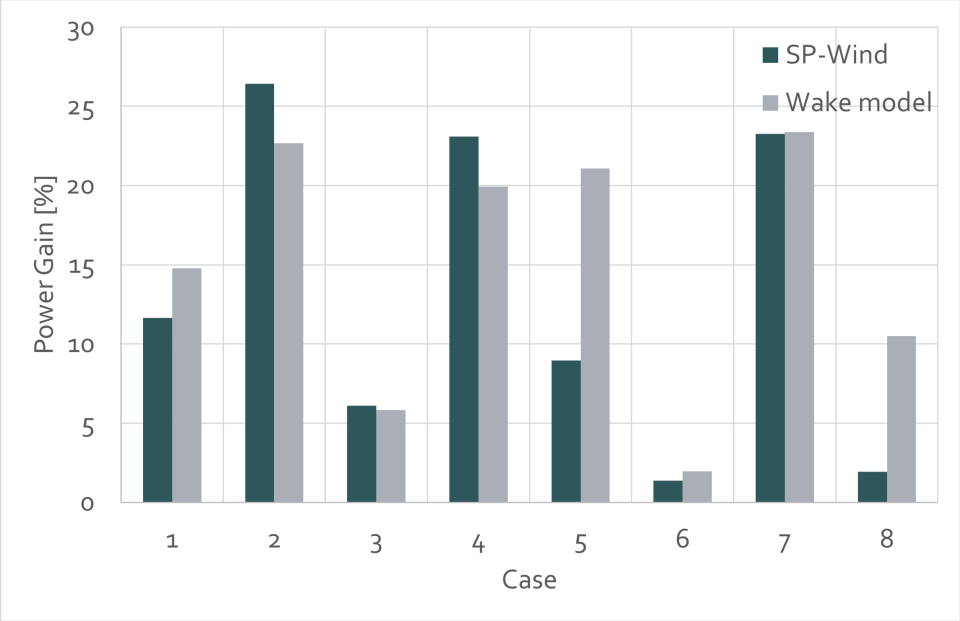

Fig. 4 Comparison of total wind farm power gains predicted by the wake model versus power gains obtained from SP-Wind using optimal yawing set-points.

and θ_0 a reference temperature. The effect of the sea surface is included using a wall-stress model, corresponding to a logarithmic velocity profile with a roughness length z_0 [19]. Finally, $\bar{\mathbf{F}}$ represents body forces on the flow.
Spatial discretization in SP-Wind is performed by combining pseudo-spectral schemes in the span-wise and stream-wise directions, with fourth-order energy-conservative finite differences in the vertical direction.The equations are marched in time using a fully explicit fourth-order Runge–Kutta scheme, and grid parallellization is achieved through a scalable pencil decomposition approach. Subgrid-scale stresses are modeled with a standard Smagorinsky model with Mason and Thomson wall damping [18]. Wind turbines are modeled by an actuator sector model, coupled with a nonlinear flexible multi-body dynamics model [20]. Turbulent inflow conditions for wind farm simulations are generated in a concurrent precursor simulation, which are then introduced in the wind farm domain by means of body forces in a fringe region [21]. The simulations are run in 2 steps: First, a spin-up period of 15 min is initiated for the settling of start-up transients, followed by 60 minutes of data collection. The LES time step is set to 0.5s, while the structural solver operates at a higher frequency of 100 Hz. The general domain parameters for the LES simulations are outlined in Table 2, and the simulation domain is shown in Figure 3.

V. Results and discussion

A comparison of the power gains reported by the analytical model and SP-Wind are shown in Figure 4 and a comparison of the average flow fields between the original reference cases and the optimally yawed cases for the Lillgrund wind farm and TC RWP are presented in Figures 5 and 6 respectively. As previously discussed, both cases 2 and 7 have fully aligned turbines for the TC RWP and the Lillgrund wind farm respectively, hence have a high capacity for power gains by steering the upstream turbine wakes away from downstream wakes, which can also be observed from the time averaged flow field results from SP-Wind. Figure 4 shows a direct consequence of wake steering, exhibiting power gains up to 25% for both the TC RWP and the Lillgrund wind farm. For six of the eight cases, the power gains obtained via the high fidelity SP-Wind code are in good agreement with the predictions made by the low fidelity wake model, with cases 5 and 8 exhibiting larger errors. This can be attributed to two factors. First, the turbulence intensity model used in the wake model is an empirical expression proposed by Niayifar and Porté-Agel [22], that has been tuned for the range of $0.065 < TI < 0.15$, and fails to accurately capture the power generation of the extreme farm layout in case 5 with eight aligned turbines and TI of 3.6%. Second, the wake expansion and recovery downstream of yawed turbines also depends on empirical parameters which need to be tuned for different wind farm layouts and wind speeds, and currently the model fails to accurately predict the power production at the low wind speed and tight layout

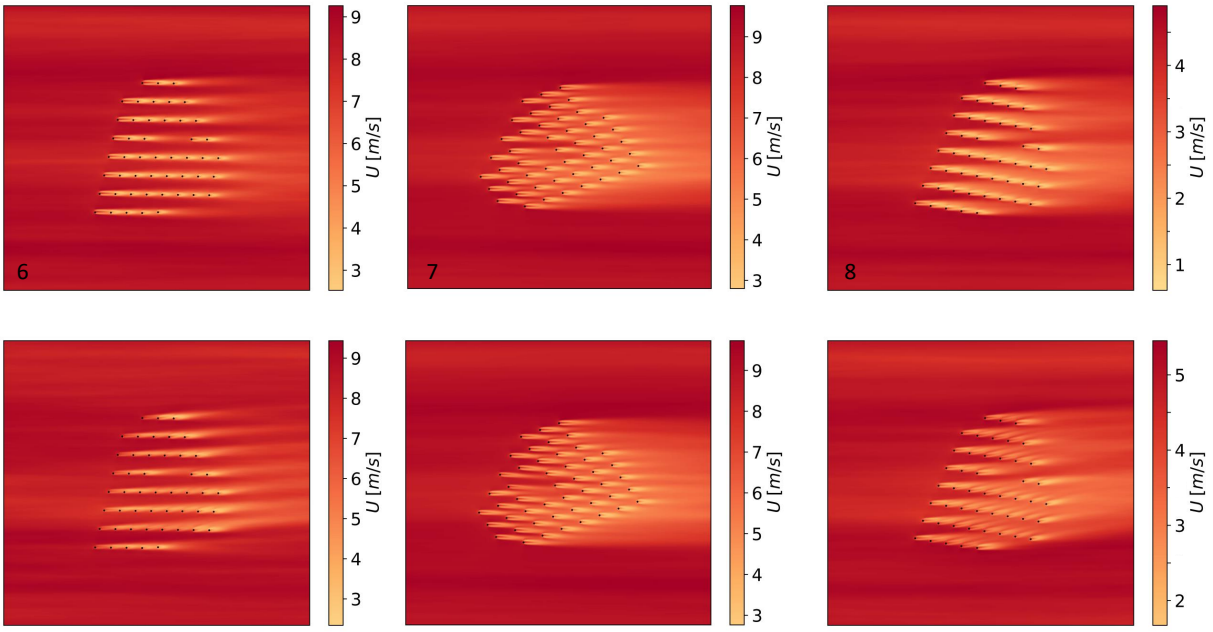

Fig. 5 Comparison of average flow fields obtained from SP-Wind for the reference cases (top) and simulations with optimal yaw set-points (bottom) for the Lillgrund wind farm.

configuration of the Lillgrund wind farm for case 8, in which majority of the wind turbines are operating in partial waked conditions. Thus, the results provided by the wake model model can further be improved by calibration and tuning the empirical parameters involved to cover a larger range of turbulence intensities and farm layouts as suggested in literature [7], however that is beyond the scope of the current work. Nevertheless, the yaw set-points obtained in both these cases from the optimization still result in significant power gains when tested in the high fidelity environment of SP-Wind, resulting in power gains of 9% and 2% respectively.

To determine the effect of wake steering on the structure of the turbines, we use Damage Equivalent Loads (DELs) to evaluate the increase in fatigue in the optimal wake steering cases against normal operation. DEL of each turbine is computed using the Palmgren–Miner rule and the Wöhler equation to account for accumulating fatigue damage caused to the wind turbine components by the fluctuating structural loads [23].The loads time series are counted and binned into individual cycles using the rainflow-counting algorithm [24], and for the wind turbine blades the components follow the Wöhler's curve with a slope coefficient equal to 10 . Total increase in cumulative wind farm blade root flap-wise DEL is shown in Figure 7. It can observed that for all the cases, the wind farm experiences significant increase in damage due to fatigue. The reason for increase in damage can be explained by two factors. First, individual turbines are subjected to higher fatigue loads while operating in yawed position than when compared to normal operation [25]. Second, in certain cases downstream turbines are operating in partially waked conditions leading higher cyclic fluctuations in moments, thus increasing the fatigue damage. Hence, while wake steering can result in an increase in overall wind farm power production, it is important to do a cost benefit analysis when using this control strategy due to the large impact on the structural lifetime of the turbines due to increased fatigue loading.

VI. Conclusions

In this work, a recursive wake merging methodology is utilized to develop an optimization framework for determining optimal yaw set-points in two wind farms operating under varying atmospheric conditions. The resulting yaw set-points are then tested in a high fidelity LES environment to validate the power gains predicted by the analytical model. Of the eight cases simulated, a good comparison between LES and the analytical model is obtained in terms of relative power gains, however larger errors in certain cases which have deep wind turbine arrays or lower inflow turbulent

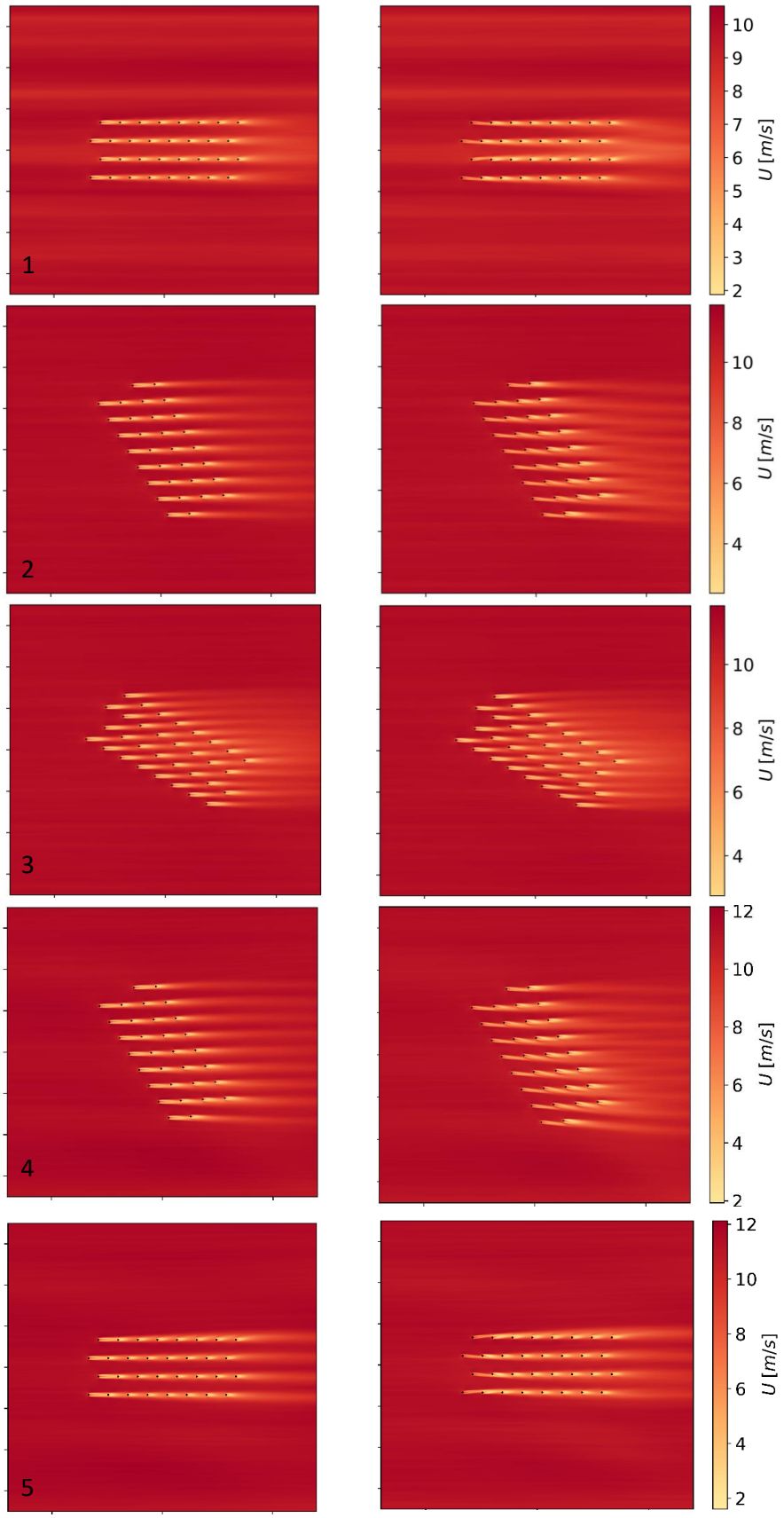

Fig. 6 Comparison of average flow fields obtained from SP-Wind for the reference cases (left) and simulations with optimal yaw set-points (right) for the TC RWP.

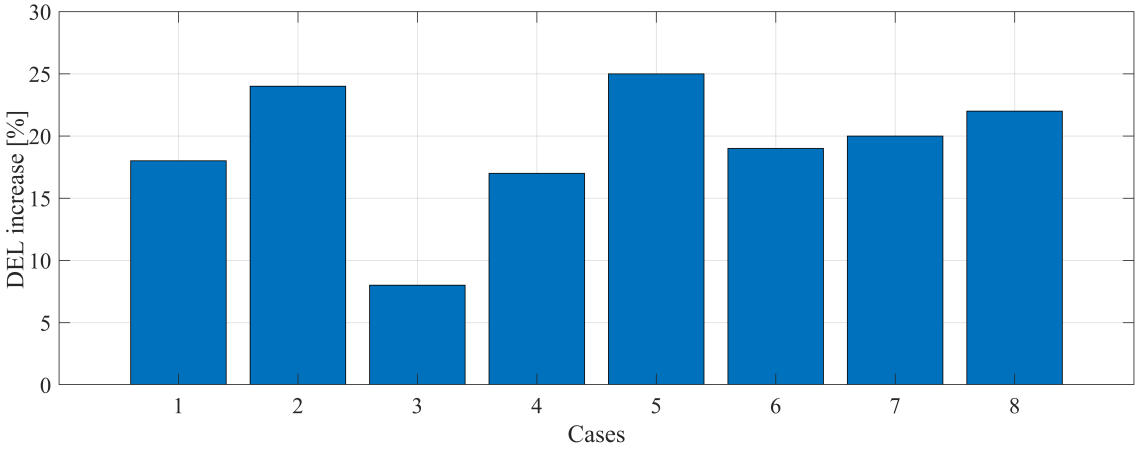

Fig. 7 Comparison of total wind farm flap-wise DEL increase due to optimal wake steering for power optimization.

intensity is observed. A direct consequence of yawing the turbines to boost power production is also observed through increased structural fatigue in the wind turbine blades. Therefore, future work could include a cost benefit analysis in the optimization framework, by penalizing the increase in structural loads through wind farm control. Additionally, the performance of the analytical model could be improved by model tuning. Nevertheless, the set-points obtained still result in significant power gains up to 25% when tested in the LES setup, exhibiting the benefits of the developed optimization framework.

Acknowledgments

The authors have received funding from the European Unions Horizon 2020 programme (TotalControl, grant no. 727680). The computational resources and services used in this work were provided by the VSC (Flemish Supercomputer Center), funded by the Research Foundation Flanders (FWO) and the Flemish Government department EWI.

References

[1] Boersma, S., Doekemeijer, B. M., Gebraad, P. M., Fleming, P. A., Annoni, J., Scholbrock, A. K., Frederik, J. A., and Van Wingerden, J. W., "A tutorial on control-oriented modeling and control of wind farms," *Proceedings of the American Control Conference*, 2017, pp. 1–18. https://doi.org/10.23919/ACC.2017.7962923.

[2] Annoni, J., Gebraad, P. M. O., Scholbrock, A. K., Fleming, P. A., and Wingerden, J.-W. v., "Analysis of axial-induction-based wind plant control using an engineering and a high-order wind plant model," *Wind Energy*, Vol. 19, No. 6, 2016, pp. 1135–1150. https://doi.org/https://doi.org/10.1002/we.1891, URL https://onlinelibrary.wiley.com/doi/abs/10.1002/we.1891.

[3] Munters, W., and Meyers, J., "Dynamic strategies for yaw and induction control of wind farms based on large-eddy simulation and optimization," *Energies*, Vol. 11, No. 1, 2018. https://doi.org/10.3390/en11010177.

[4] Bastankhah, M., and Porté-Agel, F., "Experimental and theoretical study of wind turbine wakes in yawed conditions," *Journal of Fluid Mechanics*, Vol. 806, 2016, pp. 506–541. https://doi.org/10.1017/jfm.2016.595.

[5] Lanzilao, L., and Meyers, J., "A new wake-merging method for wind-farm power prediction in the presence of heterogeneous background velocity fields," *Wind Energy*, 2021. https://doi.org/10.1002/we.2669.

[6] Pavel, H., "Cubature formulas for the unit disk," , 2011. URL http://www.holoborodko.com/pavel/numerical-methods/numerical-integration/cubature-formulas-for-the-unit-disk/.

[7] Doekemeijer, B. M., van der Hoek, D., and van Wingerden, J. W., "Closed-loop model-based wind farm control using FLORIS under time-varying inflow conditions," *Renewable Energy*, Vol. 156, 2020, pp. 719–730. https://doi.org/10.1016/j.renene.2020.04.007, URL https://doi.org/10.1016/j.renene.2020.04.007.

[8] Virtanen, P., Gommers, R., Oliphant, T. E., Haberland, M., Reddy, T., Cournapeau, D., Burovski, E., Peterson, P., Weckesser, W., Bright, J., van der Walt, S. J., Brett, M., Wilson, J., Millman, K. J., Mayorov, N., Nelson, A. R. J., Jones, E., Kern, R., Larson, E., Carey, C. J., Polat, İ., Feng, Y., Moore, E. W., VanderPlas, J., Laxalde, D., Perktold, J., Cimrman, R., Henriksen, I., Quintero, E. A., Harris, C. R., Archibald, A. M., Ribeiro, A. H., Pedregosa, F., van Mulbregt, P., and SciPy 1.0 Contributors, "SciPy 1.0: Fundamental Algorithms for Scientific Computing in Python," *Nature Methods*, Vol. 17, 2020, pp. 261–272. https://doi.org/10.1038/s41592-019-0686-2.

[9] Anderson, S. J., Meyers, J., Sood, I., and Troldborg, N., "TotalControl D 1.04 Flow Database for reference wind farms," , 2020.

[10] Simisiroglou, N., Polatidis, H., and Ivanell, S., "Wind farm power production assessment: a comparative analysis of two actuator disc methods and two analytical wake models," *Wind Energy Science*, Vol. 2018, No. February, 2018, pp. 1–13. https://doi.org/10.5194/wes-2018-8.

[11] Munters, W., Sood, I., and Meyers, J., "Precursor dataset PDk," , Apr. 2019. https://doi.org/10.5281/zenodo.2650100, URL https://doi.org/10.5281/zenodo.2650100.

[12] Munters, W., Sood, I., and Meyers, J., "Precursor dataset PDkhi," , Apr. 2019. https://doi.org/10.5281/zenodo.2650102, URL https://doi.org/10.5281/zenodo.2650102.

[13] Munters, W., Sood, I., and Meyers, J., "Precursor dataset CNk2," , Apr. 2019. https://doi.org/10.5281/zenodo.2650096, URL https://doi.org/10.5281/zenodo.2650096.

[14] Munters, W., Sood, I., and Meyers, J., "Precursor dataset CNk4," , Apr. 2019. https://doi.org/10.5281/zenodo.2650098, URL https://doi.org/10.5281/zenodo.2650098.

[15] Goit, J. P., and Meyers, J., "Optimal control of energy extraction in wind-farm boundary layers," *Journal of Fluid Mechanics*, Vol. 768, 2015, pp. 5–50. https://doi.org/10.1017/jfm.2015.70.

[16] Allaerts, D., and Meyers, J., "Gravity Waves and Wind-Farm Efficiency in Neutral and Stable Conditions," *Boundary-Layer Meteorology*, Vol. 166, No. 2, 2018, pp. 269–299. https://doi.org/10.1007/s10546-017-0307-5.

[17] Munters, W., Meneveau, C., and Meyers, J., "Turbulent Inflow Precursor Method with Time-Varying Direction for Large-Eddy Simulations and Applications to Wind Farms," *Boundary-Layer Meteorology*, Vol. 159, No. 2, 2016, pp. 305–328. https://doi.org/10.1007/s10546-016-0127-z.

[18] Allaerts, D., and Meyers, J., "Large eddy simulation of a large wind-turbine array in a conventionally neutral atmospheric boundary layer," *Physics of Fluids*, Vol. 27, No. 6, 2015. https://doi.org/10.1063/1.4922339, URL http://dx.doi.org/10.1063/1.4922339.

[19] Bou-Zeid, E., Meneveau, C., and Parlange, M., "A scale-dependent Lagrangian dynamic model for large eddy simulation of complex turbulent flows," *Physics of Fluids*, Vol. 17, No. 2, 2005, pp. 1–18. https://doi.org/10.1063/1.1839152.

[20] Vitsas, A., and Meyers, J., "Multiscale aeroelastic simulations of large wind farms in the atmospheric boundary layer," *Journal of Physics: Conference Series*, Vol. 753, No. 8, 2016, p. 082020. https://doi.org/10.1088/1742-6596/753/8/082020, URL https://iopscience.iop.org/article/10.1088/1742-6596/753/8/082020.

[21] Stevens, R. J., Graham, J., and Meneveau, C., "A concurrent precursor inflow method for Large Eddy Simulations and applications to finite length wind farms," *Renewable Energy*, Vol. 68, 2014, pp. 46–50. https://doi.org/10.1016/j.renene.2014.01.024, URL http://dx.doi.org/10.1016/j.renene.2014.01.024.

[22] Niayifar, A., and Porté-Agel, F., "Analytical modeling of wind farms: A new approach for power prediction," *Energies*, Vol. 9, No. 9, 2016, pp. 1–13. https://doi.org/10.3390/en9090741.

[23] Sutherland, "Fatigue analysis of wind turbines. Technical report, Sandia National Laboratories," Tech. rep., 1999.

[24] Socie, D., and Downing, S., "Simple Rainflow Counting Algorithms," *International Journal of Fatigue*, Vol. 4, No. 1, 1982, pp. 31–40. URL http://masters.donntu.org/2015/fimm/zinchencko/library/article11.pdf.

[25] Damiani, R., Dana, S., Annoni, J., Fleming, P., Roadman, J., van Dam, J., and Dykes, K., "Assessment of wind turbine component loads under yaw-offset conditions," *Wind Energy Science*, Vol. 3, No. 1, 2018, pp. 173–189. https://doi.org/10.5194/wes-3-173-2018, URL https://wes.copernicus.org/articles/3/173/2018/.